AN IMPROVED CARBON DIOXIDE SNOW SPECTRAL ALBEDO MODEL: APPLICATION TO MARTIAN CONDITIONS

D. Singh (sdeepak@umich.edu)[1], and M.G. Flanner[1]
[1]Climate and Space Sciences and Engineering, University of Michigan, Ann Arbor, Michigan, USA

Introduction:

The Martian atmosphere consists primarily of carbon dioxide, and Martian polar caps are covered primarily with carbon dioxide ice [*Leighton and Murray*, 1966; *Herr and Pimentel*, 1969; *Larson and Fink*, 1972; *Forget*, 1998; *Bibring* et al., 2005]. H_2O ice is also present at the surface of the perennial ice caps, with small amounts of seasonal deposition in other parts of the planet [e.g., *Kieffer* et al., 2000; *Brown* et al., 2014]. Significant portions of atmospheric CO_2 (25-30%) deposit seasonally in each hemisphere, as indicated by model simulations and surface pressure measurements [*Tillman* et al., 1993; *Forget* et al., 1998; *Kieffer and Titus*, 2001]. To understand the impact of these ices on the planet's cryosphere albedo, it is important to accurately determine the spectral dependence of CO_2 snow albedo and influences of properties such as dust content, ice grain size, and snow thickness, as well as the albedo effects of mixing and layering of CO_2 and H_2O snow.

Our work determines the albedo of CO_2 snow by extending the Earth-based Snow, Ice, and Aerosol Radiation (SNICAR) model [*Flanner* et al., 2007; *Flanner* et al., 2009], originally designed for H_2O snow. SNICAR utilizes the multiple scattering, multi-layer two-stream radiative approximation described by *Toon* et al. [1989], with the delta-hemispheric mean approximation. We extend the current version of SNICAR from 470 bands (over the wavelength range 0.3-5.0 μm) to 480 bands spanning 0.2-5.0 μm at 10 nm spectral resolution. We include these extra 10 bands in the ultraviolet (UV) spectrum because of the lack of ozone in the Martian atmosphere compared to Earth [*Montmessin and Lefèvre*, 2013], meaning more UV radiation reaches the Martian surface and interacts with snow. A single-layer implementation of SNICAR can be operated interactively on the web at: *http://snow.engin.umich.edu*.

Very few studies have focused on modeling of Martian CO_2 snow albedo across the UV, visible and near-IR spectrum [*Warren* et al., 1990; *Hansen*, 1999]. *Langevin et al*., [2007] and *Appéré et al.*, [2011] present modeled near-IR albedo of Martian cryospheric surfaces, as discussed in Section 4. With the availability of more accurate and spectrally-resolved laboratory measurements of CO_2 ice complex refractive indices across the solar spectrum [*Hansen*, 1997; *Hansen* 2005], we provide improved and updated spectral albedos of carbon dioxide snow with applicability to Martian conditions. The presence of light-absorbing impurities generally lowers snow albedo. We simulate the impact of Martian dust [*Wolff* et al., 2006; *Wolff* et al., 2009; *Wolff* et al., 2010] and palagonite [*Clark* et al., 1990; *Clancy* et al., 1995] on surface cryosphere albedo. Palagonite is a volcanic rock and serves as a terrestrial analog for Martian dust [*Banin* et al., 1997]. We perform multiple analyses to determine the sensitivity of cryosphere spectral albedo to the amount and type of dust, presence of both ices, ice grain size, snow layer thickness, and solar zenith angle. We also compare our simulations with observed Mars surface albedo derived from Compact Reconnaissance Imaging Spectrometer (CRISM) measurements, and the OMEGA instrument [*Appéré et al.*, 2011].

Data and Methodology:

Hansen [1997, 2005] made extensive laboratory measurements of the complex refractive indices of solid CO_2 ice in the spectral range from 0.174 μm to 333 μm. We apply these data along with Mie calculations to derive optical properties of different lognormal size distributions of CO_2 ice particles, reported with effective radius (r_{eff}), or the surface area-weighted mean radius of the size distribution. Our simulations of H_2O snow albedo utilize refractive indices of H_2O ice provided by *Warren and Brandt* [2008]. We use "central hematite" dust mineral fractions from *Balkanski* et al. [2007] as a proxy of typical Earth dust. These mineral abundances are representative of aeolian dust from the Saharan desert. Refractive indices for this dust mixture are derived using the Maxwell-Garnett mixing approximation, following e.g., *Sokolik and Toon* [1999], along with measurements of mineral refractive indices from various sources. Refractive indices of Martian dust (hereafter Mars dust) were provided by Mike Wolff (Space Science Institute, personal communication), and were derived using data from instruments onboard the Mars Reconnaissance Orbiter (MRO), as described by *Wolff* et al. [2009], and *Wolff* et al. [2010]. We combine refractive indices of palagonite from *Clark* et al. [1990] over the 0.2 μm to 0.6 μm spectral range and measurements from 0.6 μm to 5 μm made by *Clancy* et al. [1995] to derive data over the solar spectrum. In this study, we divide our broadband (0.2-5.0 μm) into two sub-regions: Visible (0.2-0.7 μm) and near-IR (0.7-5.0 μm).

We determine the spectrally-varying single scatter albedo (ω_0), scattering asymmetry parameter (g), and mass extinction cross-section for all three dust types using Mie Theory with an assumed gamma size distribution [*Hansen and Travis*, 1974] with r_{eff}=1.5μm and effective variance (υ_{eff})=0.3 [*Wolff* et

al., 2006]. Figure 1 shows the optical properties for these dust types. Mass absorption cross-section (Fig. 1d) is the product of single scatter co-albedo (Fig. 1a) and mass extinction cross-section (Fig 1b).

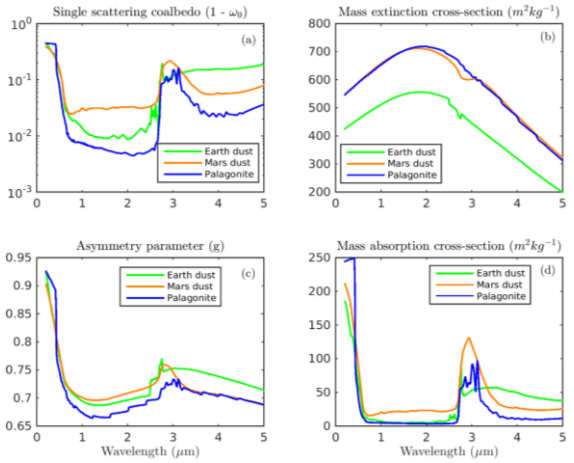

Figure 1: Spectral optical properties of the Earth dust, Martian dust, and palagonite applied in this study.

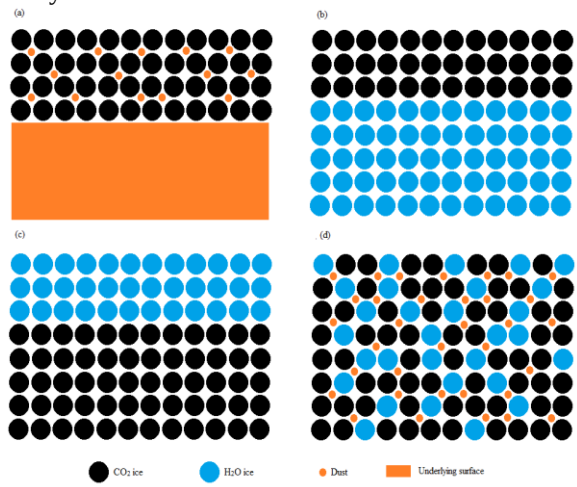

Figure 2: Schematic of the various model configurations applied in this paper: (a) a single CO_2 or H_2O snow layer (with dust) on top of solid underlying surface; (b) CO_2 snow with variable thickness on top of a semi-infinite H_2O snow layer; (c) H_2O snow with variable thickness on top of a semi-infinite CO_2 snow layer; (d) mixed snow layers with dust.

The bulk optical properties (extinction optical depth (τ), ω_0, and g) for each snow layer are calculated from the abundances of each constituent [e.g., *Flanner* et al, 2007], with τ calculated as the sum of that associated with each constituent, ω_0 as a τ-weighted average of each constituent, and *g* as a scattering optical depth (product of τ and ω_0) weighted average of the asymmetry parameter of each constituent. These bulk layer properties are then applied in the two-stream multiple scattering approximation adopted by SNICAR. We utilize this extended framework of SNICAR to first simulate the albedo of pure CO_2 snow across the visible and near-IR spectrum. We then explore and compare the impacts of Earth dust, Mars dust and palagonite on CO_2 and H_2O snow albedo. Finally, we adopt a two layer model (with the bottom layer being semi-infinite) to calculate the impacts of H_2O snow presence on top of CO_2 snow and vice-versa. In all other cases we assume only a single snow layer, either with semi-infinite thickness or varying shallow thicknesses. Here, a layer with thickness of 100 m is referred to as semi-infinite. Figure 2 shows simplified diagrams of the various model configurations applied in this paper.

Results:

We have simulated the spectral albedo of CO_2 snow using an enhanced 480-band version of SNICAR, which was previously developed for terrestrial snow. We explored CO_2 snow albedo across the entire solar spectrum, including UV, visible and near-IR wavelengths. Our analysis shows significant differences between H_2O and CO_2 snow albedos. H_2O snow is about 8 times more absorptive than CO_2 snow in the near-IR region, and 7 times more absorptive averaged over the entire solar spectrum. Figure 3 shows the spectral hemispheric albedo of pure, semi-infinite CO_2 and H_2O snow with spherical grain effective radius of 100 µm and solar zenith angle of 60°. It is evident that the CO_2 is more reflective than H_2O snow, especially in the near-IR spectrum. CO_2 snow albedo shows very little dependence on solar zenith angle and a weaker dependence on grain size than H_2O snow. The broadband albedo of CO_2 snow decreases by only 0.064 as effective grain size increases from 50 to 1500 µm.

The presence of thin snow layers exposes underlying surfaces to incoming radiation, hence impacting the surface albedo. The saturation thicknesses for CO_2 snow and H_2O snow range from approximately 6.5 – 100 cm and 5 – 83 cm, respectively, for effective grain sizes ranging from 50 to 1500 µm, though we caution again that these thicknesses may be smaller with non-spherical ice particles. Non-spherical grains scatter less strongly in the forward direction, thereby decreasing the penetration depth of solar radiation. Thicker CO_2 snow is required to negate the impact of underlying surface because CO_2 ice grains scatter more strongly than H_2O ice grains, especially in the near-IR spectrum. The presence of 0.01% dust reduces the broadband albedo of CO_2 snow by about 50%, with Martian dust being the darkest type of dust explored here, followed by typical Earth dust and palagonite (Figure 4). The spectral shape of albedo changes caused by palagonite, which is often used as a Martian dust analog, closely follow those of Mars dust, but palagonite is not as absorptive as Mars dust. The impact of dust on CO_2 snow albedo saturates after its mass mixing ratio exceeds roughly 0.1%.

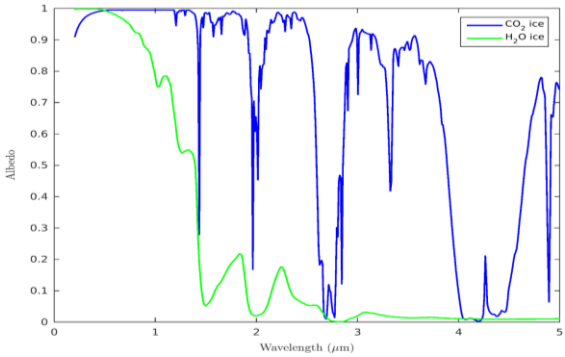

Figure 3: Comparison of CO_2 and H_2O snow spectral albedo simulated with the SNICAR model (Grain size = 100 μm and solar zenith angle = 60°)

Because of the contrasting properties of H_2O and CO_2 ice in the near-IR spectrum, different layering and mixing configurations of these types of snow can have substantial impact on net surface albedo. With an effective grain size of 100 μm, only about 2.5 cm of H_2O snow is needed to mask the influence of underlying CO_2 snow on net surface albedo (Table 5), while more than double this amount of CO_2 snow is needed to mask the influence of H_2O snow (Table 6). Such effects are relevant for the perennial H_2O ice caps of Mars, and where water vapor from the atmosphere condenses on top of CO_2 ice in other areas of the planet. When both snow types are present as a mixture rather than separate layers, 0.01% of H_2O snow reduces the broadband albedo of CO_2 snow by 0.03, while 1% of CO_2 snow is required to increase the broadband albedo of H_2O snow by the same amount.

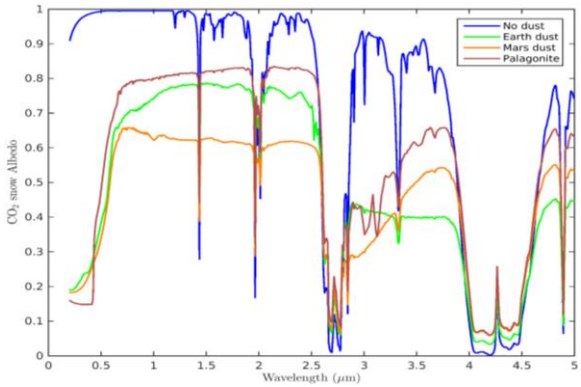

Figure 4: Impact of different types of dust on CO_2 snow albedo, with dust mass mixing ratio of 0.01%. The assumed snow grain size is 100 μm.

With the identification of optimal snow parameter combinations, our results show a decent agreement between modeled spectral albedo and observed reflectance of the Martian polar ice caps in the 1–4 μm spectral range. The CRISM data exhibit anomalously high reflectance at 2.7 μm, which cannot be explained with presence of either CO_2 or H_2O ice, as both media are highly absorptive at this wavelength (Figure 5). SNICAR also provides realistic best-fit parameters for matching OMEGA near-IR observations (Figure 6), though the spectral fit is not as good as that achieved previously with a directional reflectance model [*Appéré et al.*, 2011]. Simulations presented here could potentially be used in combination with observed data to refine the calibration of surface albedo retrieval algorithms. Model results can also be used to interpolate measurements to higher spectral resolution. The new spectrally resolved albedos for CO_2 snow presented here have potentially wide applicability to any planet or system with CO_2 ice, especially Mars.

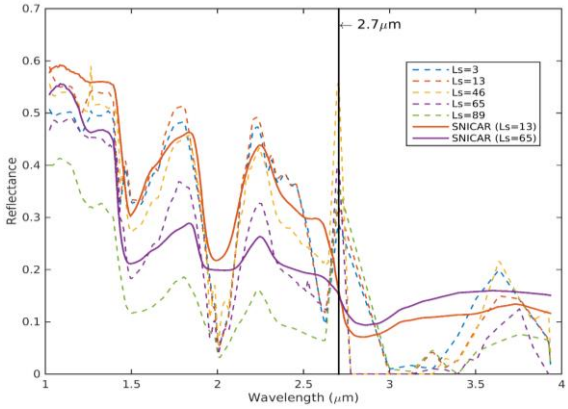

Figure 5: Observed reflectance for location N (dotted curves) along with modeled albedo using best-fit parameters (solid blue curve). The black vertical line at 2.7 μm indicates the outlier.

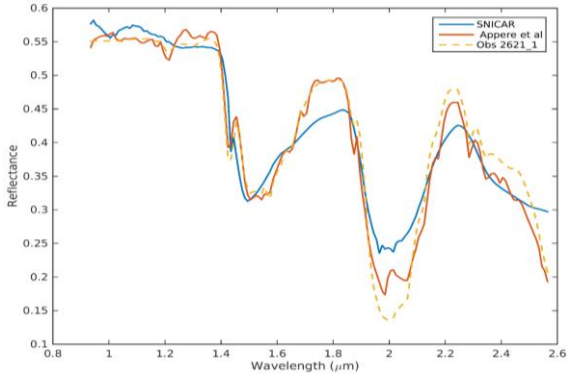

Figure 6: Comparison of best fit albedo using SNICAR and the model applied by *Appéré et al.*, [2011] against data from OMEGA observation 2621_1.

References:

Appéré, T., et al. (2011), Winter and spring evolution of northern seasonal deposits on Mars from OMEGA on Mars Express, J. Geophys. Res., 116, E05001, doi:10.1029/2010JE003762.

Balkanski, Y., M. Schulz, T. Claquin, and S. Guibert (2007), Reevaluation of Mineral aerosol radiative forcings suggests a better agreement with satellite and AERONET data. Atmospheric Chemistry and Physics, 7(1), 81-95.

Banin, A., et al. (1997), Acidic volatiles and the Mars soil, J. Geophys. Res., 102(E6), 13341–13356, doi:10.1029/97JE01160.

Bibring, J. P., et al. (2005), Mars surface diversity as revealed by the OMEGA/Mars Express observations. Science, 307(5715), 1576-1581.

Brown, A. J., S. Piqueux, and T. N. Titus, (2014), Interannual observations and quantification of summertime H_2O ice deposition on the Martian CO_2 ice south polar cap. Earth and Planetary Science Letters, 406, 102-109.

Clancy, R. T., S. W. Lee, G. R. Gladstone, W. W. McMillan, and T. Roush (1995), A new model for Mars atmospheric dust based upon analysis of ultraviolet through infrared observations from Mariner 9, Viking, and Phobos, J. Geophys. Res., 100, 5251– 5264.

Clark, R. N., T. V. King, M. Klejwa, G. A. Swayze, and N. Vergo (1990), High spectral resolution reflectance spectroscopy of minerals. J. Geophys. Res., 95(B8), 12653–12680, doi:10.1029/JB095iB08p12653.

Flanner, M. G., C. S. Zender, J. T. Randerson, and P. J. Rasch (2007), Present day climate forcing and response from black carbon in snow, J. Geophys. Res., 112, D11202, doi:10.1029/2006JD008003.

Flanner, M. G., et al. (2009), Springtime warming and reduced snow cover from carbonaceous particles, Atmos. Chem. Phys., 9, 2481-2497.

Forget, F. (1998), Mars CO_2 ice polar caps. In Solar System Ices, Springer Netherlands, 477-507.

Forget, F., F. Hourdin, and O. Talagrand (1998), CO_2 snowfall on Mars: Simulation with a general circulation model. Icarus, 131(2), 302-316.

Hansen, G. B. (1997), The infrared absorption spectrum of carbon dioxide ice from 1.8 to 333 μm, J. Geophys. Res., 102(E9), 21569–21587, doi:10.1029/97JE01875.

Hansen, G. B. (1999), Control of the radiative behavior of the Martian polar caps by surface CO_2 ice: Evidence from Mars Global Surveyor measurements, J. Geophys. Res., 104(E7), 16471–16486, doi:10.1029/1998JE000626.

Hansen, G. B. (2005), Ultraviolet to near-infrared absorption spectrum of carbon dioxide ice from 0.174 to 1.8 μm. J. Geophys. Res., 110, E11003, doi:10.1029/2005JE002531.

Hansen, J. E., and L. D. Travis (1974), Light scattering in planetary atmospheres. Space Science Reviews, 16(4), 527-610.

Herr, K. C., and G. C. Pimentel (1969), Infrared absorptions near three microns recorded over the polar cap of Mars. Science, 166(3904), 496-499.

Kieffer, H. H., and T. N. Titus, (2001), TES mapping of Mars' north seasonal cap. Icarus, 154(1), 162-180.

Kieffer, H. H., et al. (2000), Mars south polar spring and summer behavior observed by TES: Seasonal cap evolution controlled by frost grain size, J. Geophys. Res., 105(E4), 9653–9699, doi:10.1029/1999JE001136.

Langevin, Y., J.-P. Bibring, F. Montmessin, F. Forget, M. Vincendon, S. Douté, F. Poulet, and B. Gondet (2007), Observations of the south seasonal cap of Mars during recession in 2004–2006 by the OMEGA visible/near-infrared imaging spectrometer on board Mars Express, J. Geophys. Res., 112, E08S12, doi:10.1029/2006JE002841.

Larson, H. P., and U. Fink (1972), Identification of carbon dioxide frost on the Martian polar caps. The Astrophysical Journal, 171, L91.

Leighton, R. B., and B. C. Murray (1966), Behavior of carbon dioxide and other volatiles on Mars. Science, 153(3732), 136-144.

Montmessin, F., and F. Lefèvre (2013), Transport-driven formation of a polar ozone layer on Mars. Nature geoscience, 6(11), 930-933, doi:10.1038/ngeo1957.

Sokolik, I. N., and O. B. Toon (1999), Incorporation of mineralogical composition into models of the radiative properties of mineral aerosol from UV to IR wavelengths, J. Geophys. Res., 104(D8), 9423–9444, doi:10.1029/1998JD200048.

Tillman, J. E., N. C. Johnson, P. Guttorp, and D. B. Percival (1993), The martian annual atmospheric pressure cycle: Years without great dust storms. Journal of Geophysical Research: Planets (1991–2012), 98(E6), 10963-10971.

Toon, O. B., C. P. McKay, T. P. Ackerman, and K. Santhanam (1989), Rapid calculation of radiative heating rates and photodissociation rates in inhomogeneous multiple scattering atmospheres, J. Geophys. Res., 94 (D13), 16287-16301, doi:10.1029/JD094iD13p16287.

Warren, S. G., W. J. Wiscombe, and J. F. Firestone (1990), Spectral albedo and emissivity of CO_2 in Martian polar caps: Model results, J. Geophys. Res., 95(B9), 14717–14741, doi:10.1029/JB095iB09p14717.

Warren, S. G., and R. E. Brandt (2008), Optical constants of ice from the ultraviolet to the microwave: A revised compilation, J. Geophys. Res., 113, D14220, doi:10.1029/2007JD009744.

Wolff, M. J., R. T. Clancy, J. D. Goguen, and M. C. Malin, and B. A. Cantor (2010), Ultraviolet dust aerosol properties as observed by MARCI. Icarus, 208(1), 143-155.

Wolff, M. J., et al. (2009), Wavelength dependence of dust aerosol single scattering albedo as observed by the Compact Reconnaissance Imaging Spectrometer, J. Geophys. Res., 114, E00D04, doi:10.1029/2009JE003350.

Wolff, M.J. et al. (2006), Constraints on dust aerosols from the Mars Exploration Rovers using MGS overflights and Mini-TES. J. Geophys. Res., 111, E12S17, doi:10.1029/2006JE002786.